

DISTRIBUTED MAXIMUM POWER POINT TRACKING WITH OVERVOLTAGE PROTECTION FOR PV SYSTEMS

SEGUIMIENTO DISTRIBUIDO DEL PUNTO DE MÁXIMA POTENCIA CON PROTECCIÓN DE SOBREVOLTAJE

CARLOS ANDRÉS RAMOS-PAJA

Ph.D., Profesor Facultad de Minas, Universidad Nacional de Colombia, Sede Medellín, caramosp@unal.edu.co

ANDRÉS JULIÁN SAAVEDRA-MONTES

Ph.D., Profesor Facultad de Minas, Universidad Nacional de Colombia, Sede Medellín, ajsaaved@unal.edu.co

MASSIMO VITELLI

Doctor, Dip. Ingegneria dell'Informazione, Second University of Naples, Aversa (CE), Italy, vitelli@unina.it

Received for review July 4th, 2012, accepted October 9th, 2012, final version October, 11th, 2012

ABSTRACT: This paper presents an integral solution of the overvoltage problem caused by mismatched conditions when DC-DC converter outputs of PV systems are connected in series, and a distributed maximum power point tracking architecture is implemented. The operating conditions that cause the overvoltage problem are discussed in detail and the consequences of the overvoltage problem are illustrated. The proposed solution is based on a structure that includes a non-linear controller, two linear controllers, and a maximum power point tracking algorithm. Such a solution makes it possible to regulate the PV voltage according to the MPPT controller commands and to limit the DC-DC converter output voltage to avoid damages. The non-linear control structure is experimentally validated with a boost converter and a BP585 PV panel. Simulation results show that the proposed integral solution allows the operation of PV panels in the feasible maximum power point and protects the integrity of the DC-DC converters, avoiding the overvoltage problem caused by mismatched conditions.

KEYWORDS: photovoltaic systems, DC-DC converters, overvoltage protection, distributed maximum power point tracking

RESUMEN: Este artículo presenta una solución integral al problema de sobrevoltaje en sistemas fotovoltaicos, el cual aparece cuando las salidas de los convertidores DC-DC de sistemas fotovoltaicos se conectan en serie y simultáneamente se implementa una estructura de seguimiento distribuido del punto de máxima potencia. Las condiciones de operación que causan el sobrevoltaje en las salidas de los convertidores DC-DC se discuten en detalle a la vez que se ilustran las consecuencias del problema. La solución propuesta está basada en una estructura que incluye un controlador no lineal, dos controladores lineales y un algoritmo de seguimiento del punto de máxima potencia. Esta solución regula el voltaje de los paneles fotovoltaicos, sigue el punto de máxima potencia y limita el voltaje de salida del convertidor DC-DC para evitar la destrucción del mismo. La estructura de control no lineal es validada experimentalmente utilizando un convertidor elevador y un panel fotovoltaico BP585. Los resultados de simulación muestran que la solución integral propuesta en este artículo permite la operación de paneles fotovoltaicos en los puntos de máxima potencia factibles y mantiene la integridad de los convertidores DC-DC a través de la protección de sobrevoltaje.

PALABRAS CLAVE: sistemas fotovoltaicos, convertidores DC-DC, protección de sobrevoltaje, seguimiento distribuido del punto de máxima potencia

1. INTRODUCTION

Solar energy, and in particular Photovoltaic (PV) power systems, are one of the promising technologies to reduce pollution caused by oil-based generators, providing redundancy in critical applications and *in situ* energy generation, among other residential and portable applications [1-4].

Due to the low voltage of PV panels, PV applications commonly adopt step-up power converters to achieve the higher voltage requirements of the load or grid-connected inverter [5]. In addition, traditional PV solutions use PV arrays composed by series connected PV panels to increase the voltage provided to the power converter [6]. However, differences in the operating conditions of the panels cause the mismatching phenomenon, *e.g.* when shadows affect one or some

PV modules of a series PV array. This phenomenon strongly reduces the total power production. This is mainly due to different irradiation levels causing multiple peaks, or local maximums, in the power-voltage characteristic of a series connected PV array, which opens the possibility that classical Maximum Power Point Tracking (MPPT) algorithms being trapped in a non-absolute power maximum [6]. The mismatching phenomenon is also caused by a series connection of PV panels with different electrical characteristics, which is the case of replacing damaged panels when an identical replacement is not available. Also, mismatching conditions are generated by the integration of PV panels in urban environments, where the available area forces different panel orientations.

The new frontier in PV technology is to avoid the power drops generated by such mismatching conditions. One of the most promising solutions is the use of switching converters dedicated to each PV module [6]. Solutions based on DC-DC converters [7] or DC-AC converters [8] have been proposed. The most adopted solution is the use of DC-DC converters as a first stage, since it makes possible to efficiently supply DC loads and also, by means of an additional DC-AC converter it can supply AC loads or inject energy into the grid [9]. Moreover, in such a grid-connected double stage architecture is possible to add features such as power factor correction [5].

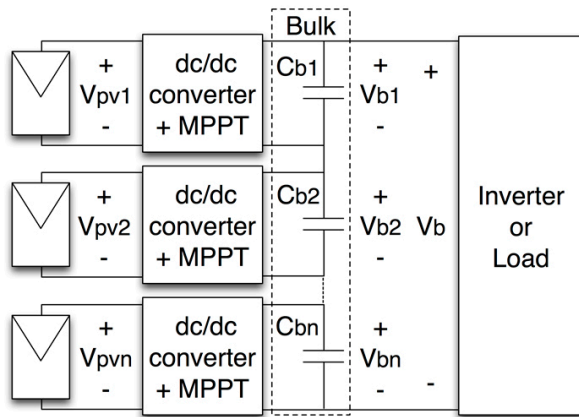


Figure 1. DMPPT for step-up PV systems.

The architecture based on a DC-DC converter for each PV module also permits Maximum Power Point (MPP) tracking in each panel, removing the local power maximums and leaving a single absolute one. Such architecture, depicted in figure 1, is known as

Distributed Maximum Power Point Tracking (DMPPT) [6]. However, the DMPPT creates new problems related to the series connection of the DC-DC converter outputs: noise transmission between the DC-DC converters, interference between the simultaneous MPPT controllers, high-side semiconductor driving in typical low-side DC-DC topologies, and overvoltage caused by mismatched conditions that could destroy the DC-DC converters. The noise transmission problem has been addressed by using a voltage controller to mitigate the converter's output effect on the PV voltage [5, 9]. The interference problem has been addressed by designing multi-output DMPPT algorithms to asynchronously perturb each PV voltage, isolating the effect of a single panel from the other ones [6]. The high-side driving problem is an intrinsic characteristic of the series connection, which can be avoided by using isolated MPPT controllers, but such solution is not applicable in PV systems with synchronized DMPPT algorithms used to reduce interference between MPPT controllers [6]. The potentially destructive overvoltage problem has been slightly discussed in literature [6], but practical solutions are difficult to find.

The overvoltage problem to identify safe operating conditions is discussed in detail in Sections 2 and 3. In Section 4, a solution based on a non-linear/linear control structure is proposed, which makes possible to regulate the PV voltage in agreement with the MPPT controller commands, and to limit the DC-DC converter output voltage to avoid damages. Finally, conclusions presented in Section 5 close the paper.

2. PV PANEL ELECTRICAL BEHAVIOR

The single diode model, presented in figure 2 [10], is an accepted representation of the photovoltaic and ohmic effects that define the PV panel's electrical behavior. Such a model is described by the non-linear equation given in (1), where I_{PV} and V_{PV} are current and voltage of the panel, R_s and R_h are the series and parallel resistances of the model, $V_d = V_{PV} + I_{PV} \cdot R_s$ is the voltage of the diode model and I_O its inverse saturation current. n is the ideal factor of the P-N junction, k is the Boltzmann constant, q is electron charge, and T_{PV} is the panel temperature in kelvins. Finally, I_{ph} is the current produced by the photovoltaic effect.

$$I_{PV} = I_{ph} - I_O \left[\exp \left(\frac{V_{PV} + I_{PV} \cdot R_s}{n \cdot k \cdot T_{PV} / q} \right) - 1 \right] - \frac{V_d}{R_h} \quad (1)$$

The photovoltaic and inverse saturation currents depend on both the solar irradiance and the panel temperature as in (2) [11], where the sub-index STC refers to measurements at Standard Test Conditions [10, 11], G is the solar irradiance, V_{OC} is the PV panel open circuit voltage, *i.e.* $I_{PV} = 0$, and α_i and α_v are the current and voltage thermal coefficients. Such parameters can be extracted from manufacturers' datasheets [11].

$$\begin{aligned}
 I_{ph} &= I_{ph,STC} (G / G_{STC}) + \alpha_i (T_{PV} - T_{STC}) \\
 I_O &= I_{ph} \cdot \exp[-q \cdot V_{OC} / (n \cdot k \cdot T_{PV})] \\
 V_{OC} &= V_{OC,STC} + \alpha_v (T_{PV} - T_{STC})
 \end{aligned}
 \tag{2}$$

But the implicit solution of such a non-linear model (1) requires a complex calculation process based on the Lambert W function as described in [10]. Moreover, such an implicit model is not suitable for control purposes, therefore simpler linear models have been adopted in literature to represent the PV panel around its optimal operating point: Norton, Thevenin, and differential resistance models. In [9], it was demonstrated the improved accuracy and features of the Norton model, presented in figure 2, in terms of control. Such a model is described by the PV short circuit current, $V_{PV} = 0$, and its impedance at the MPP.

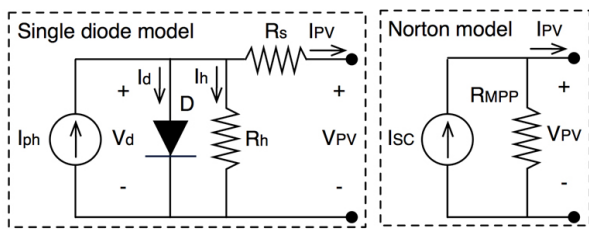


Figure 2. Non-linear and linear PV models.

Figure 3 shows the electrical characteristics of a BP585 PV panel [11] for different operating conditions, where it is noted that an optimum operating point MPP, where the PV delivers the maximum power, exist for each irradiance and temperature. Figure 3(a) presents the non-linear behavior of the PV current and power (P_{PV}) for different irradiance conditions at constant temperature, where the Norton model parameters at such MPPs are also observed: short circuit current (I_{SC}) and R_{MPP} . It is noted that I_{SC} increases with the irradiance G while R_{MPP} decreases for the same condition. Figure 3(b) presents a similar analysis for changes in the panel temperature, where I_{SC} decreases for decrements on T_{PV} while R_{MPP} increases. From both

figures, 3(a) and 3(b), it is noted that the MPP position (V_{MPP} and I_{MPP}) changes for both G and T_{PV} , while the maximum power (P_{MPP}) increases for higher G and lower T_{PV} . Finally, figure 3(c) shows the behavior of V_{MPP} , I_{SC} and R_{MPP} for variations on both G and T_{PV} ; it is evident that a MPPT controller is required to track online the V_{MPP} operating condition; and the Norton model parameters significantly change depending on the environmental conditions, which is an important condition for the control system.

3. LIMITATIONS ON DMPPT OPERATING CONDITIONS

Taking into account the DMPPT structure, depicted in figure 1, it is noted that the power systems composed by a PV panel and an associated DC-DC converter with an output capacitor C_{bi} , are all in series. Therefore, the current that flows between the output ports of such systems, *i.e.* C_{bi} capacitors terminals, is the same current defined by the load I_b . In addition, since a PV panel optimal operating condition depends on its irradiance and temperature, defined by the optimal PV voltage (V_{MPP}), the existence of mismatching conditions among panels imposes different input voltage for the DC-DC converters associated with the mismatched panels. Moreover, mismatched panels provide lower power than non-mismatched ones, and the associated DC-DC converters deliver less power to the load than those of non-mismatched panels.

Assuming that identical DC-DC converters form a DMPPT system, which is an actual design condition if the PV panels are from the same reference as in traditional cases, the power losses of each DC-DC converter will be approximately the same. In such conditions, the power delivered to the load by a DMPPT system of n PV panels, figure 1, is given by (3), where P_b is the total power delivered to the load, $P_{b1} \dots P_{bn}$ represent the power delivered by each DC-DC converter, and whose voltages $V_{b1} \dots V_{bn}$ compose the bulk voltage V_b .

$$\begin{aligned}
 P_b &= P_{b1} + P_{b2} \dots + P_{bn} = \sum_{i=1}^n P_{bi} \\
 V_b &= V_{b1} + V_{b2} \dots + V_{bn} = \sum_{i=1}^n V_{bi}
 \end{aligned}
 \tag{3}$$

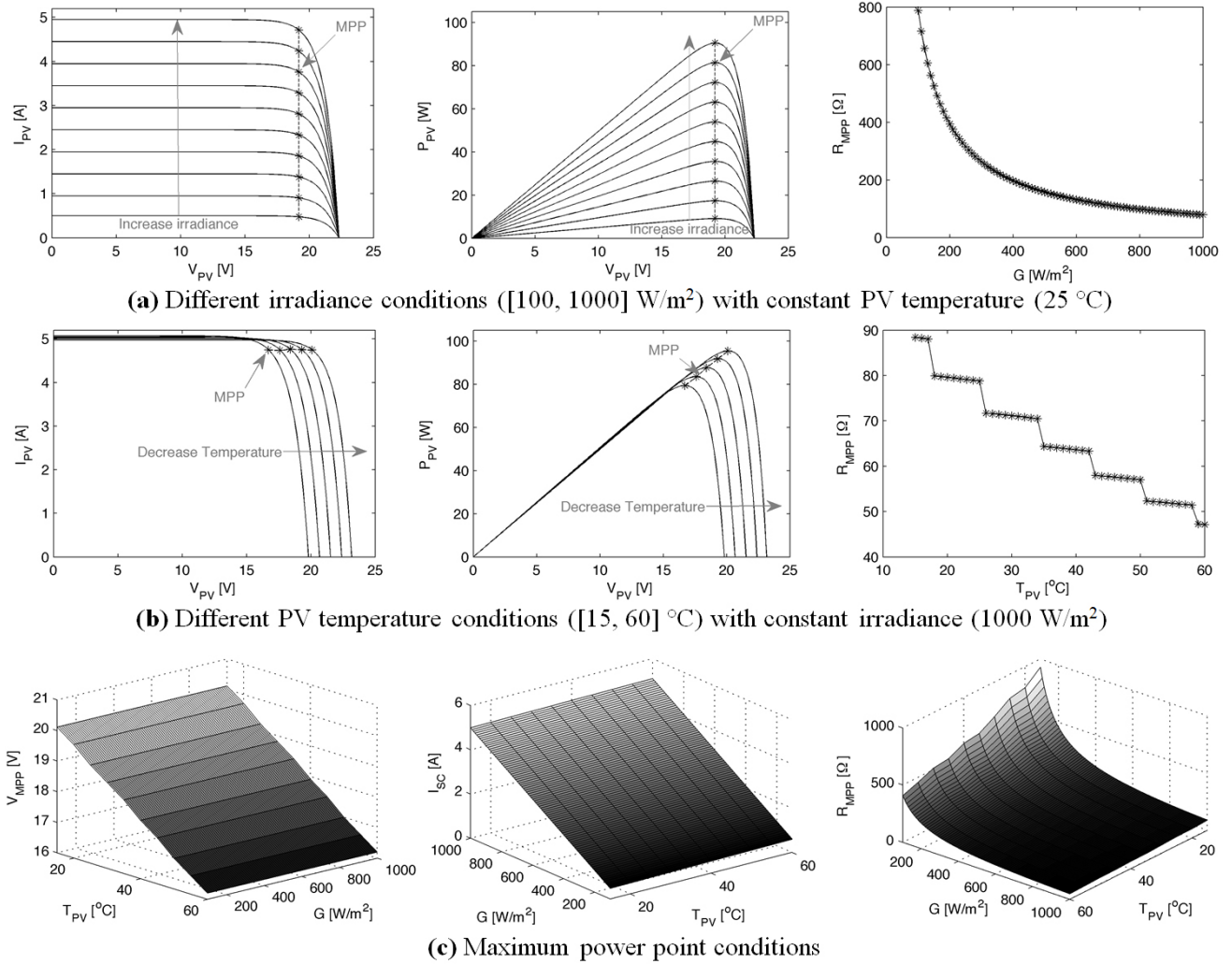


Figure 3. BP585 electrical behavior

From (3), the output voltage of each DC-DC converter is given by (4). If the PV array has uniform conditions, *i.e.* no mismatching, all panels provide the same power and the output voltages are equal $V_{b1} = V_{b2} = \dots = V_{bn} = V_b/n$.

$$V_{bi} = V_b \cdot P_{bi} / P_b \quad (4)$$

But in mismatched conditions, the DC-DC converters that provide higher power will exhibit higher output voltages, which could lead to damage of the output capacitor and/or semiconductors. For example, for two BP585 with $G_1 = G_2 = 1000 \text{ W/m}^2$ and an imposed bulk voltage $V_b = 90 \text{ V}$, the DC-DC converters output voltages are $V_{b1} = V_{b2} = 45 \text{ V}$. A cost-effective design requires output capacitors with commercial voltage ratings of 50 V , which support the required voltage at

the minimum cost. In boost converters the last analysis is also valid for the MOSFET, which supports the given output voltage. In buck-boost converters, the MOSFET supports the sum of input and output voltages, *i.e.* $V_{PVi} + V_{bi}$, therefore a semiconductor with commercial rating of 70 V is required. But if mismatching conditions appear, for example shadowing in one panel $G_2 = 500 \text{ W/m}^2$, the output voltages are different: $V_{b1} = 60 \text{ V}$ and $V_{b2} = 30 \text{ V}$. In such a condition, the capacitor and MOSFET, for both boost and buck-boost, of the first DC-DC converter will be destroyed since the maximum ratings are exceeded.

Moreover, if the mismatching unbalance is high enough, the non-mismatched system will assume all the bulk voltage. For example, in a DMPPT system with ten panels and an imposed $V_b = 380 \text{ V}$, the commercial

voltage rating in uniform conditions for C_{b1} is 50 V, while the MOSFET rating is 50 V for boost converters and 65 V for buck-boost converters. However, if six panels have an irradiance $G_1 = 1000 \text{ W/m}^2$ and four mismatched panels have $G_2 = 200 \text{ W/m}^2$, the behavior is different for buck-boost and boost systems. In buck-boost systems, the non-mismatched DC-DC converters exhibit output voltages equal to 55.88 V, which destroy both output capacitors that support 55.88 V and MOSFETs that support approximately $19 \text{ V} + 55.88 \text{ V} = 74.88 \text{ V}$. In boost systems the condition is worse because the mismatched DC-DC converters exhibit output voltages equal to 11.17 V, but the MPP voltage in BP585 PV panels is near to 19 V, hence such DC-DC converters do not operate since its output voltages are higher than the input voltages. Therefore, the mismatched panels delivers even less power to the load and the associated DC-DC converters have lower output voltage, which further increases the output voltage of the non-mismatched DC-DC converters, higher than 55.88 V, and again both output capacitors and MOSFETs are destroyed.

Such limitations on the operating conditions are illustrated in figure 4 for DMPPT systems with two BP585 panels in both uniform and mismatched conditions, where $V_{b,max}$ is the output voltage limit to avoid destruction. Figure 4(a) considers boost converters, where the zones for destruction of DC-DC converters are observed, $V_{b1} > V_{b,max}$ and $V_{b2} > V_{b,max}$. Similarly, the zones for a DC-DC converters failure are also given, $V_{b1} < V_{PV1}$ and $V_{b2} < V_{PV2}$. Moreover, such figures present the power delivered to the load for safe operating conditions, where the Absolute Maximum Power Point (AMPP) is given. In uniform conditions (left), such an AMPP is feasible since $V_{b1} = V_{b2} < V_{b,max}$, but in mismatched conditions (right), the AMPP is not achievable since the C_{b1} capacitor and the associated MOSFET will be destroyed. Therefore, feasible MPPs are generated in each of the two safe operation zones of the $[V_{PV1}, V_{PV2}]$ map. In this example the right MPP has higher power than the left MPP, but it is not a general rule since the MPP's depend on the particular irradiance profiles. In a similar way, figure 4(b) presents the output voltage map of buck-boost converters, where again the AMPP is achievable in uniform conditions, but in mismatched conditions such an optimal condition, in terms of energy, damages the output capacitors and MOSFETs. The main difference between boost and

buck-boost cases is that buck-boost converters can operate in conditions where $V_{b1} < V_{PV1}$ and $V_{b2} < V_{PV2}$, therefore such regions are not present in figure 4(b).

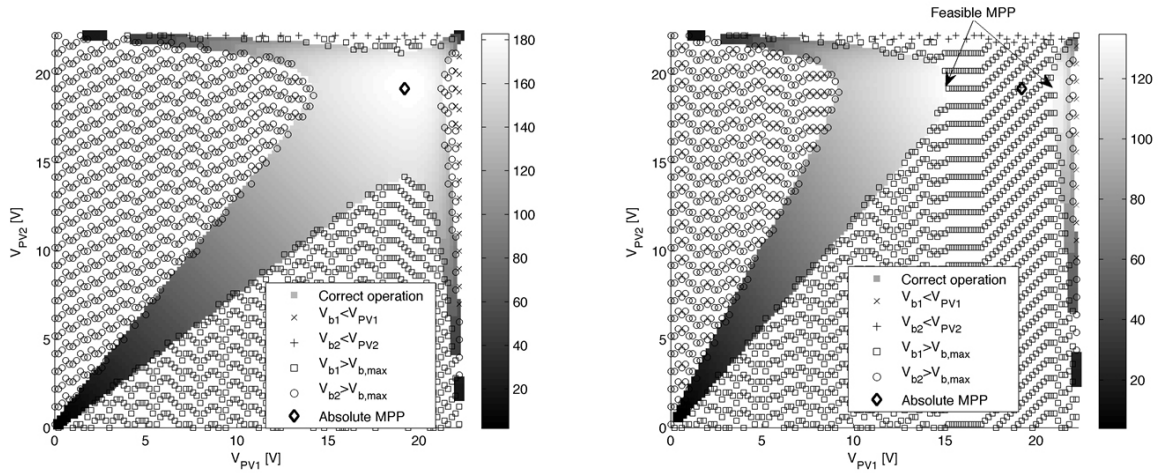
Finally, non-predictable environmental changes lead to dynamic changes of the safe operation zones of DMPPT systems, therefore an overvoltage protection is required to limit the DC-DC converters output voltage to avoid damages.

4. PV SYSTEM REGULATION

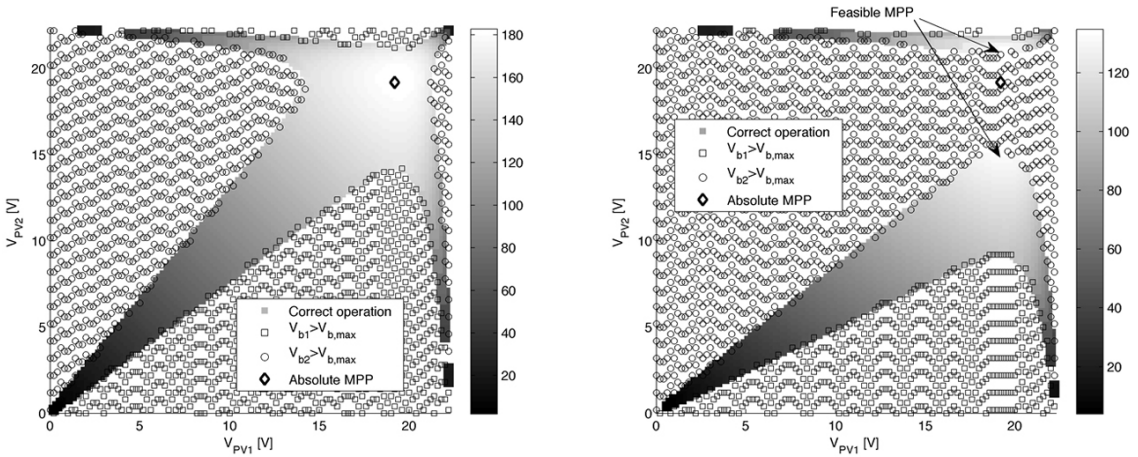
From the DMPPT operating conditions established in Sections 2 and 3, two control systems are required for the DC-DC converter: an input voltage controller to regulate the PV voltage following the reference provided by a MPPT optimization algorithm to maximize the PV power, $V_{PV} = V_{MPP}$ and an output voltage controller to limit $V_{bi} \leq V_{b,max}$ and to avoid damage of the system hardware.

Figure 5 shows the proposed control structure for each DC-DC converter of the DMPPT system, where the required two control loops are observed: an input voltage control to regulate the PV voltage, and an output voltage control to regulate the output voltage. The schematic is based on a boost converter, but the same structure is applicable to buck-boost or other DC-DC converter topologies. Moreover, in figure 5 a Norton equivalent of the bulk impedance is adopted, which is calculated from the voltage and power delivered by the DC-DC converter.

The first control condition for boost, buck-boost and other step-up or step-up/down converters, concerns the non-minimum-phase behavior of the output voltage. Such a control problem is classically addressed by performing a cascade inductor current control [12], where the design depends on the system operating point. However, as described in Section 2, the PV system strongly changes its operating condition depending on the irradiance and temperature. Therefore, this paper adopts a Sliding-Mode Controller (SMC) to regulate the inductor current. Such a non-linear controller ensures inductor current regulation for the complete operating range and not only for the designed operating point as linear controllers would.



(a) Two PV panels, boost converters (left: $G_1 = G_2 = 1000$ W/m², right: $[G_1, G_2] = [1000, 640]$ W/m²)



(b) Two PV panels, buck-boost converters (left: $G_1 = G_2 = 1000$ W/m², right: $[G_1, G_2] = [640, 1000]$ W/m²)

Figure 4. Safe DMPPT operation conditions with BP585 PV panels: $M(D) = 2$ for (a), $M(D) = 1$ for (b).

In addition, since the system has a single active device, the MOSFET, it is possible to regulate only one voltage, input or output, at a single instant. Therefore, if the $V_{bi} \leq V_{b,max}$ condition is present, the input voltage is regulated following the MPPT reference. Instead, if $V_{bi} > V_{b,max}$ occurs, the output voltage is regulated to limit it to a given safe value. Moreover, to avoid large voltage disturbances when the system switches the active control loop from input to output or from output to input, both voltage loops use the SMC as an internal loop. The following subsections describe the three loops for a boost-based PV system.

4.1. Sliding-mode inductor current controller

To regulate the inductor current i_L with a current ripple H , the sliding surface given in (5) is imposed, where i_{ref}

is the reference provided by the voltage controllers. In such a control law, the MOSFET is turned-on when $i_L < i_{ref} - H/2$, and turned-off when $i_L > i_{ref} + H/2$. The SMC implementation is given in figure 5, where a Flip-Flop avoids chattering near the commutation limits [13].

$$S(x) = i_L - i_{ref} \quad (5)$$

From the analysis of the boost converter, the differential equation in (6) is obtained, where $u = 1$ means MOSFET ON and $u = 0$ means MOSFET OFF.

$$L \frac{di_L}{dt} = v_{pvi} - v_{bi}(1-u) \quad (6)$$

In steady state conditions, i_{ref} constant, the sliding surface derivative is $dS(x)/dt = di_L/dt$. Therefore, the necessary and sufficient conditions for local surface

reachability are given in (7) [13], which are fulfilled since in a boost converter $0 < v_{pc} < v_b$.

$$\lim_{S(x) \rightarrow 0^-} \frac{dS(x)}{dt} = \frac{di_L}{dt} = \frac{v_{pvi}}{L} > 0 \text{ for } u = 1 \quad (7)$$

$$\lim_{S(x) \rightarrow 0^+} \frac{dS(x)}{dt} = \frac{di_L}{dt} = \frac{v_{pvi} - v_{bi}}{L} < 0 \text{ for } u = 0$$

Moreover, local stability exists if the equivalent continuous control input u_{eq} fulfills $0 < u_{eq} < 1$ [13]. Replacing (5) and (6) in (7), $u = u_{eq} = 1 - (v_{pvi}/v_b) + (L/v_{bi})(di_{ref}/dt)$, which leads to:

$$-\frac{v_{bi} - v_{pvi}}{L} < \frac{di_{ref}}{dt} < \frac{v_{pvi}}{L} \quad (8)$$

Since $-(v_{bi} - v_{pvi})/L$ and v_{pv}/L correspond to the inductor current slopes when the MOSFET is OFF and ON, respectively, the SMC stability and correct operation

are ensured if the current reference slope is constrained to the inductor current slope.

4.2. Voltage/current loop models

Since the inductor current is regulated by the SMC, the inductor current can be represented by a current source that imposes $i_L = i_{ref}$. The MOSFET and diode also behave as current sources that impose average currents $i_M = (1-D)i_{ref}$ and $i_D = (D)i_{ref}$, where D is the steady state duty cycle $D = 1 - V_{pv}/V_b$ [12].

The input and output capacitor currents are given in (9), and using charge balance [9, 12], the transfer functions between the SMC current reference and the input and output voltages, $G_{vpv,iref}(s)$ and $G_{vb,iref}(s)$ respectively, are given in (10).

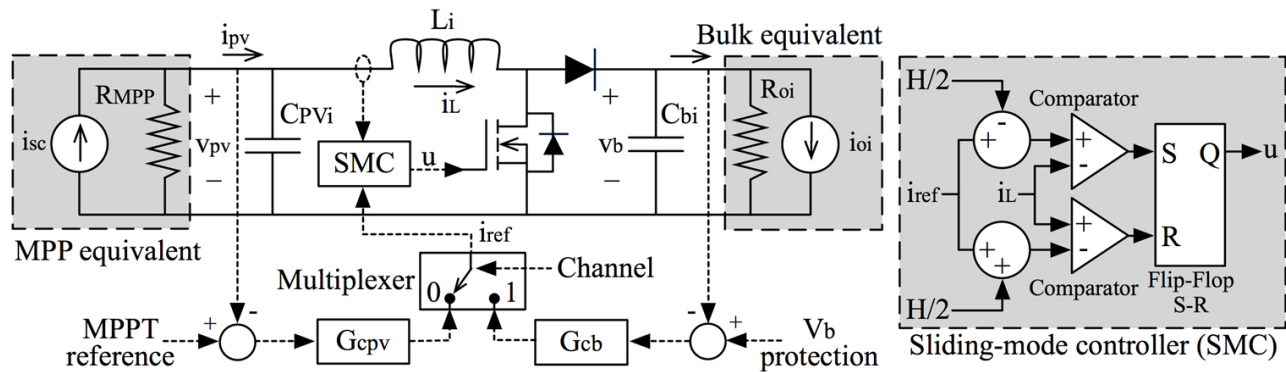


Figure 5. Proposed regulation scheme with a boost converter.

$$i_{Cpvi} = i_{sc} - v_{pv} / R_{MPP} - i_{ref} \quad (9)$$

$$i_{Cbi} = i_{ref} \cdot D - v_{bi} / R_{oi} - i_{oi}$$

$$G_{vpv,iref}(s) = \frac{v_{pv}(s)}{i_{ref}(s)} = -\frac{R_{MPP}}{R_{MPP} \cdot C_{pvi} \cdot s + 1} \quad (10)$$

$$G_{vb,iref}(s) = \frac{v_b(s)}{i_{ref}(s)} = \frac{D \cdot R_{oi}}{R_{oi} \cdot C_{bi} \cdot s + 1}$$

4.3. Voltage loop control and stability

Considering a PI controller $G_{cv}(s) = K_p + 1/(T_i \cdot s)$, and an additional gain -1 to compensate the negative term in $G_{vpv,iref}(s)$, the closed loop transfer function $T_{CL}(s)$ between voltage reference V_{ref} and PV voltage is:

$$\frac{v_{pv}(s)}{V_{ref}(s)} = \frac{R_{MPP} \cdot K_p \cdot T_i \cdot s + R_{MPP}}{R_{MPP} \cdot T_i \cdot C_{pvi} \cdot s^2 + (R_{MPP} \cdot T_i)s + R_{MPP}} \quad (11)$$

The poles of $T_{CL}(s)$ are negative for positive values of the DC-DC converter and controller parameters. Therefore, a PI controller guarantees stability of the input voltage loop. In addition, calculating the angle of the open loop transfer function $G_{loop}(s) = G_{cv}(s) \cdot G_{vpv,iref}(s)$, there is no frequency at which such an angle is equal to $-\pi$, therefore a PI controller provides infinite gain margin.

Considering $C_{pvi} = 68 \mu F$ and $C_{bi} = 100 \mu F$, $L = 100 \mu H$, $V_{MPP} = 19 V$, voltage conversion ratio $M(D) = 2$, and $R_{oi} = [(V_{MPP} \cdot M(D))^2 / P_{MPP}]$ the controller parameters $K_p = 2.9744$ and $T_i = 1.5129e-05 s$ were designed to achieve a damping factor of 0.707. In addition, the closed loop

bandwidth of the voltage controller was set to 10 kHz to limit the derivative of the reference imposed to the SMC, fulfilling the constraint given in (8).

From figure 3(c) it is noted that lower irradiances generate higher R_{MPP} , which increase $G_{vpv,ref}(s)$ gain. In such a condition the control loop $G_{loop}(s)$ gain increases, which also increases the closed loop bandwidth. To guarantee the fulfillment of (8), the voltage controller must be designed for the lowest irradiance expected, since at larger irradiances the closed loop bandwidth is reduced.

The same analysis can be applied to the output voltage, obtaining the same results due to the similarity of the transfer functions (10). In such a case, the controller parameters $K_p = 8.7480$ and $T_i = 5.1440e-06$ s were designed to obtain the same performance in terms of damping ratio and bandwidth as in the previous case. Since R_{oi} inversely depends on the power produced, lower irradiances imply higher R_{oi} , and the same conclusions are obtained: the controller must be designed for the lowest irradiance conditions.

The proposed non-linear/linear cascade control structure was experimentally validated with a boost converter, a 1/3 section of a BP585 PV panel, and an electronic load perturbing V_{bi} . Figure 6(a) shows the laboratory setup, and figure 6(b) illustrates the PV system behavior without control, where the V_{bi} perturbation propagates to the PV voltage. Instead, figure 6(c) shows the controller performance for multiple V_{bi} perturbations, which are mitigated to set the PV voltage to a given value.

Finally, figure 6(d) shows the system operating with an additional MPPT controller, which gives the reference for the PV voltage loop. In such an experiment, the MPPT, $G_{cv}(s)$ and SMC controllers ensure a three-point stable profile in the PV voltage, which guarantee the panel operation at the MPP [5]. Moreover, the control structure rejects large and fast irradiance perturbations. Such results illustrate the effectiveness of the proposed solution.

4.4. Voltage controllers switching conditions

Since the system objective is to deliver the maximum power to the load without damage, it must be operate at the feasible MPP. In such a way, when $V_{bi} \leq V_{bi,max}$,

the multiplexer channel of figure 5 must be set to 0, to force the system to follow the reference given by the MPPT controller, named MPPT mode. Instead, in the $V_{bi} > V_{bi,max}$ condition, the multiplexer channel is set to 1, and the system is regulated to keep the output voltage constant and limited, named protection mode, avoiding overvoltage conditions and damages.

4.5. Complete system performance

A DMPPT system composed by two BP585 PV panels and two boost converters was designed. Such a system follows the series structure of figure 1 and the configuration of figure 5. To illustrate the destructive overvoltage phenomenon and the proposed protection, the first DC-DC converter has the overvoltage protection disabled while the second DC-DC converter has the protection active.

To simulate real operating conditions, the non-linear PV model was considered, and the PV panels' temperatures are forced to change proportionally to the irradiance, which is a real phenomenon caused by the power dissipated in the panels [11]. In addition, the Perturb and Observe MPPT algorithm was adopted and designed as given in [5].

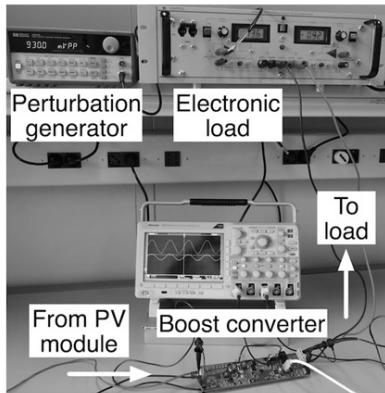
The simulation starts with uniform irradiances of 810 W/m², then at $t = 10$ ms the second panel suffers an irradiance drop to 605 W/m², causing mismatching. Previous to 10 ms both output voltages are equal since both DC-DC converters deliver the same power, and both systems operate in MPPT mode, thus exhibiting a stable three-point profile in the PV voltage. After $t = 10$ ms the output voltage of the first DC-DC converter grows due to the mismatching, reaching the voltage limit at $t = 13$ ms. From this instant the overvoltage phenomenon occurs, which destroys the first output capacitor and MOSFET in a real system. At $t = 25$ ms the irradiance of the first panel decreases to 605 W/m², and the DMPPT again reaches uniform conditions, where both PV voltages are regulated again to operate at the AMPP with a three-point stable profile. Then, at $t = 40$ ms, the irradiance of the second PV system increases again generating mismatching conditions, and at $t = 43$ ms it reaches the voltage limit.

From that instant the second system enters in protection mode, where the output voltage is regulated at the safe

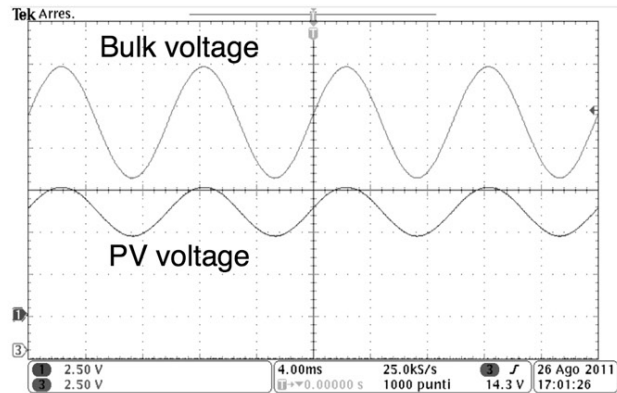
limit. In such a condition the PV voltage moves from the MPP (V_{MPP}) to reduce the power produced, reducing the relation $P_{b1}/P_{b2} = V_{b1}/V_{b2}$ as described in (3)-(4), constraining the second DC-DC converter output voltage to the desired limit. Since V_{b2} is at the safe limit and the first PV system is operating in MPPT mode, the DMPPT system reaches a feasible MPP. In addition, the MPPT algorithm stops to avoid its divergence from the vicinity of the MPP (V_{MPP}). Then, at $t = 55$ ms the irradiance of the first panel increases to 810 W/m^2 , and the DMPPT again reaches uniform conditions. In this instant, the second PV system leaves Protection mode and enters MPPT mode, therefore its PV voltage is regulated again and the DMPPT operates at the AMPP. Finally, at $t = 70$ s the irradiance of the first panel is increased to produce a shallow mismatched condition in which the protection is not activated.

5. CONCLUSIONS

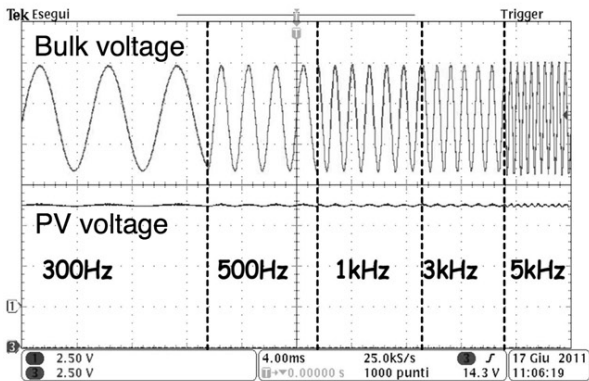
The overvoltage problem that affects PV arrays when a DMPPT structure is used and the DC-DC converter outputs are connected in series was widely illustrated in this paper. An integral solution to this problem was presented and validated based on a structure that includes a non-linear controller, two linear controllers, and a maximum power point tracking algorithm. The solution regulates the PV voltage in agreement with the MPPT controller commands and limits the DC-DC converter output voltage. The non-linear control structure was experimentally validated, and those experimental results were integrated in a simulation to validate the proposed solution.



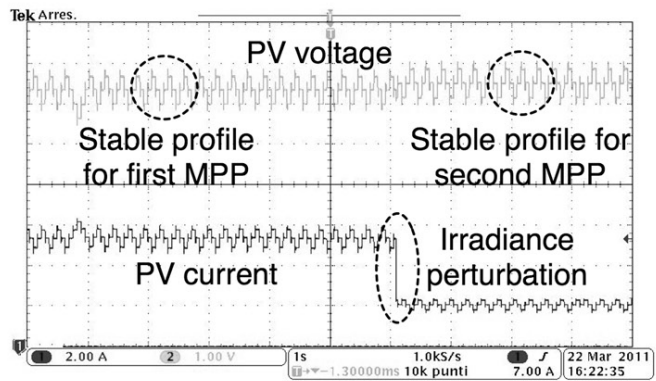
(a) Laboratory setup



(b) PV voltage without control



(c) PV voltage with proposed controllers



(d) Regulated PV system with MPPT controller

Figure 6. PV system small-signal control loop for multiple irradiance conditions.

ACKNOWLEDGEMENTS

This work was supported by SMART-ALEN and VECTORIAL-MPPT projects from *Universidad*

Nacional de Colombia and the scholarship #095-2005 from *COLCIENCIAS*.

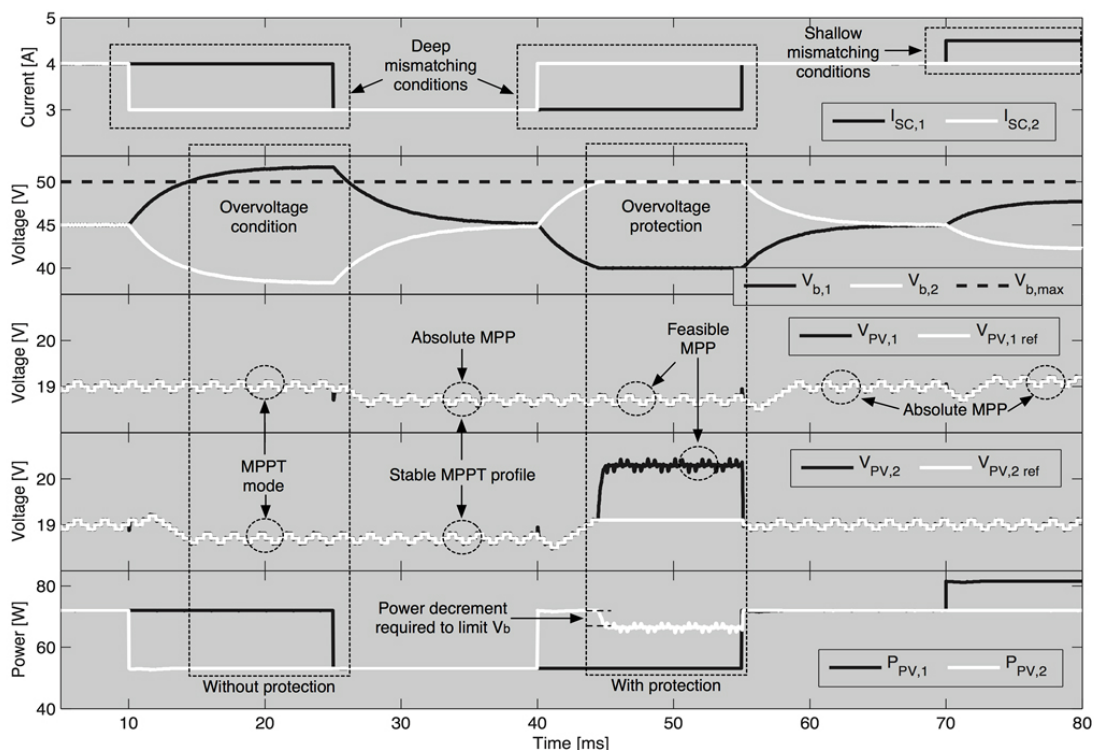


Figure 7. Dynamic performance of a DMPPT system composed by two BP585 PV panels and boost converters.

REFERENCES

- [1] Ouyang, W., Cheng, H., Zhang, X. and Yao, L., "Distribution network planning method considering distributed generation for peak cutting," *Energy Convers. Manag.*, vol. 51, pp. 2394-2401, 2010.
- [2] Benganem, M., "Low cost management for photovoltaic systems in isolated site with new IV characterization model proposed," *Energy Convers. Manag.*, vol. 50, pp. 748-755, 2009.
- [3] Soler-Bientz, R., Ricalde-Cab, L. O. and Solis-Rodriguez, L. E., "Developing a mobile stand alone photovoltaic generator," *Energy Convers. Manag.*, vol. 47, pp. 2948-2960, 2006.
- [4] Chejne, F., Macía, A., Estrada, D., Velásquez, H. and Londoño, C., "Radiation model for predicting temperature evolution in solar cooker," *Dyna*, vol. 78, pp. 68-74, 2011.
- [5] Femia, N., Petrone, G., Spagnuolo, G. and Vitelli, M., "A technique for improving P&O MPPT performances of double-stage grid-connected photovoltaic systems," *IEEE Trans. Ind. Electron.*, vol. 56, pp. 4473-4482, 2009.
- [6] Femia, N., Lisi, G., Petrone, G., Spagnuolo, G. and Vitelli, M., "Distributed maximum power point tracking of photovoltaic arrays: Novel approach and system analysis," *IEEE Trans. Ind. Electron.*, vol. 55, pp. 2610-2621, 2008.
- [7] Walker, G. and Sernia, P., "Cascaded dc-dc converter connection of photovoltaic modules," *IEEE Trans. Power Electron.*, vol. 19, pp. 1130-1139, 2004.
- [8] Li, Q. and Wolfs, P., "A review of the single phase photovoltaic module integrated converter topologies with three different dc link configurations," *IEEE Trans. Power Electron.*, vol. 23, pp. 1320-1333, 2008.
- [9] Trejos, A., Gonzalez, D. and Ramos-Paja, C. A., "Modeling of step-up grid-connected photovoltaic systems for control purposes," *Energies*, vol. 5, pp. 1900-1926, 2012.
- [10] Petrone, G., Spagnuolo, G. and Vitelli, M., "Analytical model of mismatched photovoltaic fields by means of Lambert W-function," *Sol. Energy Mater. and Sol. Cells*, vol. 91, pp. 1652-1657, 2007.
- [11] Eicker, U., "Solar technologies for buildings," John Wiley & Sons Ltd., 1st, 2003.
- [12] Erickson, R. W. and Maksimovic, D., "Fundamentals of power electronics," Springer, 2nd, 2001.
- [13] Sira-Ramirez, H., "Sliding motions in bilinear switched networks," *IEEE Trans. Circuits and Syst.*, vol. 34, pp. 919-933, 1987.